Micro-fiber reinforced cement composites. II. Flexural response and fracture studies

N. Banthia and J. Sheng

Abstract: In Part I of this paper, stress–strain curves for micro-fiber reinforced cement-based composites containing high volume fractions of carbon, steel, and polypropylene fibers were obtained. Considerable strengthening, toughening, and stiffening of the host matrix due to micro-fiber reinforcement under both static and impact conditions were reported. In this paper, composites are characterized under an applied flexural load. Both notched and unnotched specimens were tested in four-point flexure; significant improvements in the flexural behavior due to fiber reinforcement were noted. Notched specimens were tested to study the growth of cracks in these composites and to develop a valid fracture criterion. With this objective, crack growth resistance curves and crack opening resistance curves in terms of the stress intensity factor were constructed. The paper recognizes the potential of these composites in various applications and stresses the need for further research.

Key words: Portland cement-based materials, fiber reinforcement, fracture toughness, R-curves.

Résumé : Dans la première partie de cet article, des courbes contrainte–déformation pour des composites à base de ciment contenant des fractions de volume élevées de fibres de carbone, d'acier et de polypropylène ont été tracées. On a alors observé un renforcement, un durcissement et un raidissement considérables de la matrice hôte à la suite de l'addition de microfibres dans la cadre d'essais statiques et au choc. Dans cet article, les composites font l'objet d'une caractérisation à la suite de l'application d'une charge de flexion. Des éprouvettes entaillées et non encochées ont été soumises à des essais et des améliorations importantes ont été observées dans le comportement en flexion. Les éprouvettes entaillées ont fait l'objet d'une étude de propagation des fissures en vue d'élaborer un critère de rupture valide pour ces composites. À cette fin, des courbes de résistance à la propagation des fissures et des courbes de résistance à l'écartement à fond des fissures en termes de facteur d'intensité des contraintes, ont été tracées. Cet article traite des applications possibles de ces composites et souligne la nécessité de poursuivre les recherches.

Mots clés : matériaux à base de ciment Portland, renforcement par des fibres, tenacité à la rupture, courbes de résistance.
[Traduit par la rédaction]

Introduction

The high tensile strengths of asbestos–cement composites are not possible in conventionally produced fiber reinforced concretes with practically feasible volume fractions of large (macro) fibers (25–60 mm long, 0.2–1 mm in diameter) (Bentur and Mindess 1990; Balaguru and Shah 1992). When fiber volume fraction is increased in order to increase the strength in tension, severe mixing and fiber dispersion difficulties result. The real advantage of adding a nominal volume fraction of macro-fibers, however, is in the improved toughness and higher impact and fatigue resistance, which has made these composites a popular material for slabs on grade, large precast elements, and in shotcreting.

For any realistic improvement in the tensile strength, the fiber volume fraction has to be increased. It was shown in Part I of this paper (Banthia et al. 1994) that by decreasing the fiber size, a large volume fraction of fibers can be conveniently incorporated in the mix. It was also shown that with these fine (micro) fibers in the mix, a significant improvement in the uniaxial tensile strength is possible under both static and impact loadings. When under compression, however, no significant improvement in the strength was apparent. In this paper, the flexural behavior of these composites, which induces both compressive and tensile stresses in the material, is investigated. This is of particular importance, given that the most promising use of these composites is in thin sheet products which are often subjected to transverse loads.

It is sometimes believed that the intrinsic characteristics of the matrix itself are modified as a result of micro-fiber reinforcement (Beaudoin 1991; Ouyang and Shah 1992). As a result, significant improvements in the physical properties

Received July 13, 1994.
Revised manuscript accepted November 24, 1994.

N. Banthia. Department of Civil Engineering, The University of British Columbia, Vancouver, BC V6T 1Z4, Canada.
J. Sheng. Department of Civil Engineering, Laval University, Sainte-Foy, QC G1K 7P4, Canada.

Written discussion of this paper is welcomed and will be received by the Editor until December 31, 1995 (address inside front cover).

Fig. 1. Schematic of R-curve analysis.

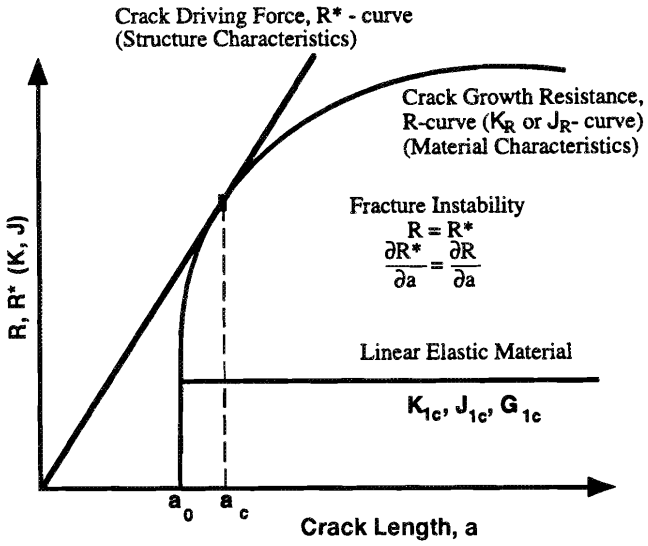

and dimensional stability of cement matrices due to micro-fiber reinforcement have been reported (Banthia et al. 1992, 1993; Banthia and Dubeau 1994). In addition to their high tensile strengths, micro-fiber reinforced composites when carrying high volume fractions of fibers are shown to depict pseudo strain hardening under tension prior to softening. In other words, after the bend over point in the stress vs. strain curve where the first matrix cracking occurs, the stresses continue to rise with a nonlinear increase in the apparent strains. It is believed that in the pseudo strain hardening regime these composites undergo significant multiple cracking and the ultimate load carrying capacity is attained only after significant matrix cracking has occurred. For a true understanding of the behavior of such composites, therefore, a fracture-based analysis is needed. Such studies not only can assist in understanding the toughening and strengthening mechanisms in these composites, but also help in establishing the much needed relation between local conditions at a crack tip and the global stresses and strains.

Crack growth resistance in fiber reinforced cement composites

Most of our modern day understanding of crack propagation in brittle materials is due to Griffith who in 1920 demonstrated that for an existing crack to grow in a linearly elastic, perfectly brittle material, a balance must exist between the increase in surface energy due to the propagation and the corresponding decrease in the potential energy of the system. In its modified form, the theory of linear elastic fracture mechanics states that an edge crack of length a in an infinite plate of ideally brittle material will propagate under an applied far-field stress, σ, when the following condition is satisfied:

$$[1] \quad K = K_c = \sigma\sqrt{\pi a}$$

where K_c is called the fracture toughness which is believed to be a material property. Notice that the theory relates the apparent strength in tension to the dimension of the critical flaw in the material such that a new design criterion, K_c, emerges.

The above analysis, although applicable to perfectly brittle materials like glass, is not valid for ductile materials like metals and quasi-brittle materials like concrete. In the case of metals, a region of plasticity develops at the tip of a loaded crack where the stresses exceed the yield strength of the material. As an approximation, if the radius of the plastic

Fig. 2. Test setup. (A notched beam under third-point flexure. A yoke surrounding the specimen eliminates the spurious system deformations from the measured beam displacements. Sensors include an LVDT mounted under the beam to measure the vertical displacement and a clip-gauge to measure the crack mouth opening displacement (CMOD).)

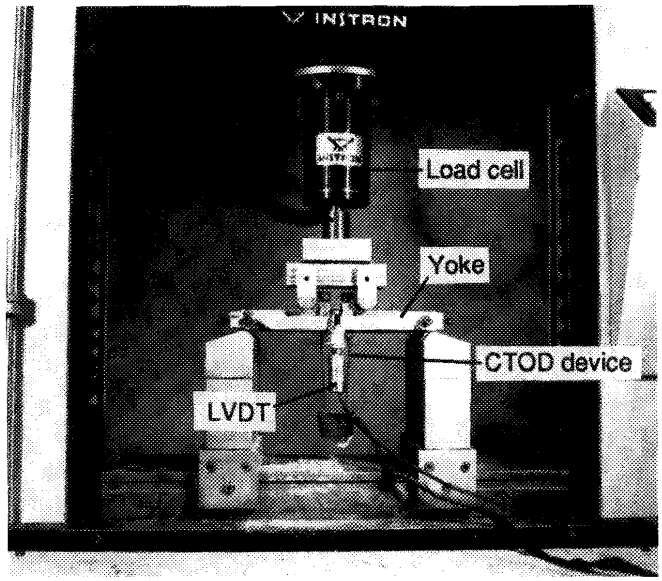

Fig. 3. Beam displacements measured with and without a yoke.

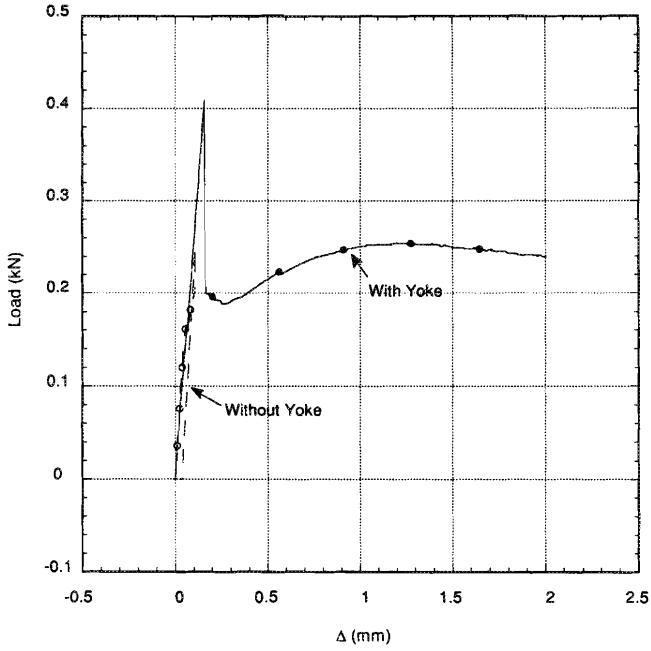

Fig. 4. Load–displacement plots for carbon fiber reinforced composite beams without a notch: (*a*) paste matrix and (*b*) mortar matrix.

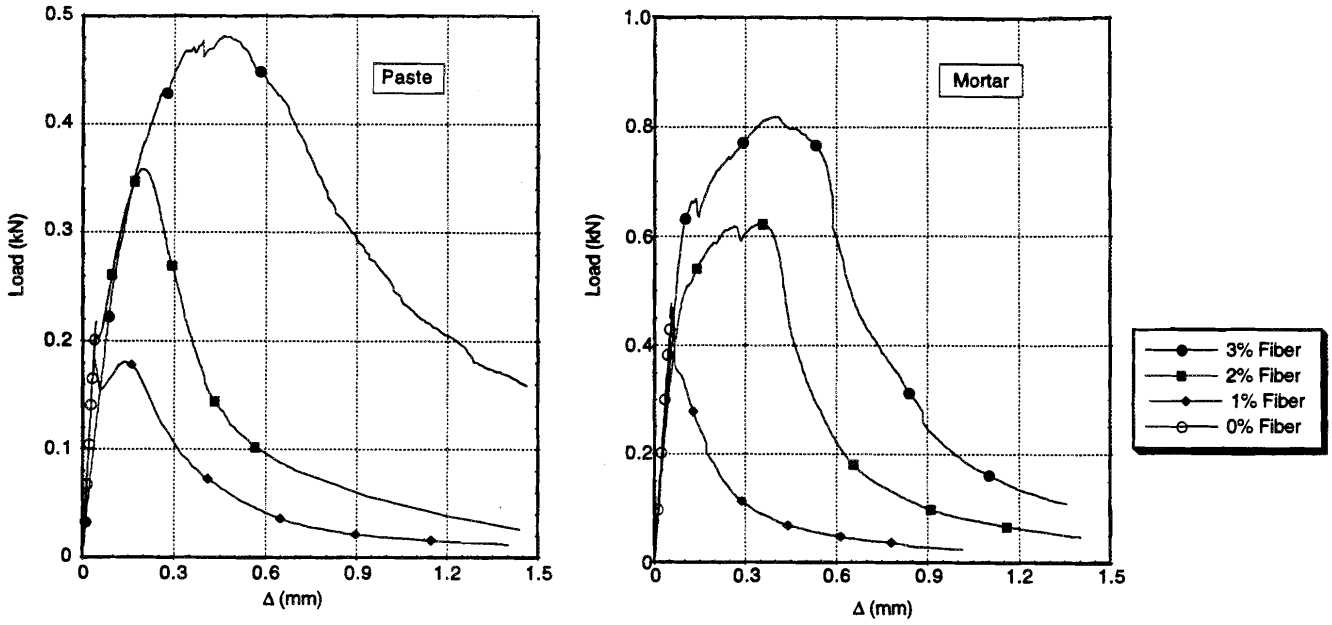

Fig. 5. Load–displacement plots for steel fiber reinforced composite beams without a notch: (*a*) paste matrix and (*b*) mortar matrix.

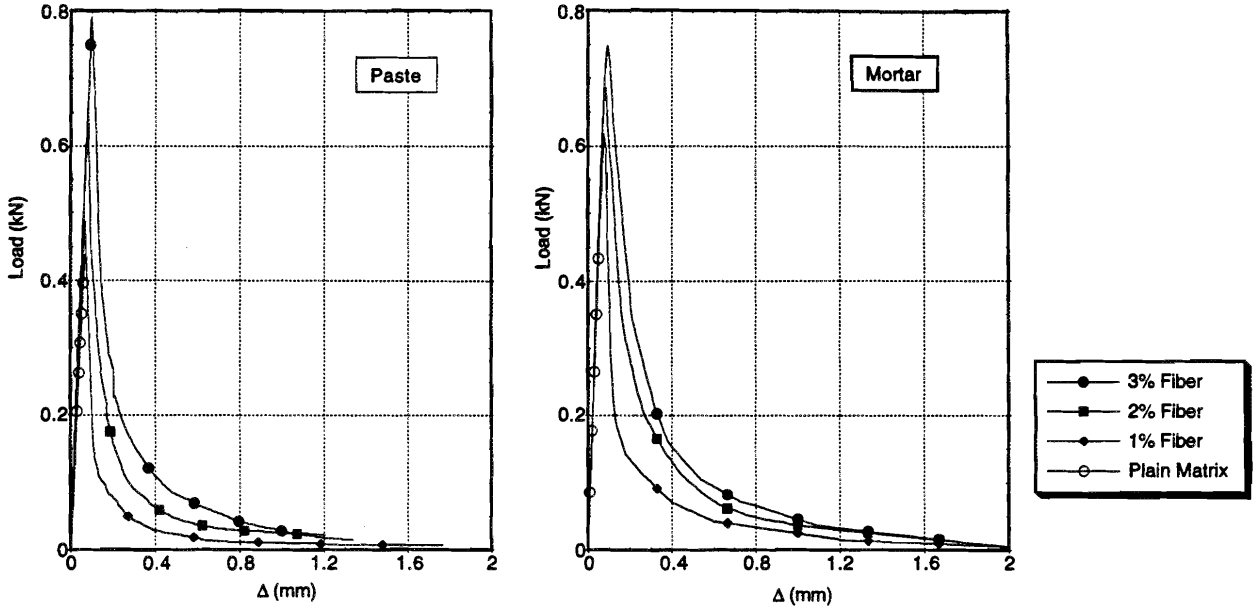

zone stays small compared with the original length of the crack, the same can be accounted for by calculating the effective fracture toughness, K_{eff}, with the effective crack length assumed to be equal to the original crack length plus some fraction of the plastic zone radius (Irwin 1958). Alternative to this equivalent elastic approach, one can reanalyze the problem of crack extension by imposing the closing pressure equal to the yield strength in the yielded portion of the crack as in Dugdale's plastic strip model (Dugdale 1960). The equivalence of these two approaches has been demonstrated (Hertzberg 1976).

In the case of concrete, considerable effort has also been made to study fracture using elastic and nonelastic fracture mechanics, and these have been extended to fiber reinforced concrete (Swamy 1979). Analogous to the plastic zone in metals, a crack process zone is created at the tip of a crack (Mindess 1991) such that the crack propagates in a stable manner before it acquires the critical dimensions needed for failure. However, while an estimation of the size of the process or yielded zone in metals is possible with reasonable accuracy, the same is not true in concrete; large variations are expected in the size of the process zone depending not only on the size and shape of the specimen but also on the loading conditions and the rate of loading. In addition, plane stress conditions can be expected to produce a process zone much larger than one produced under plane strain conditions.

Fig. 6. Load–displacement plots for polypropylene fiber reinforced composite beams without a notch: (*a*) paste matrix and (*b*) mortar matrix.

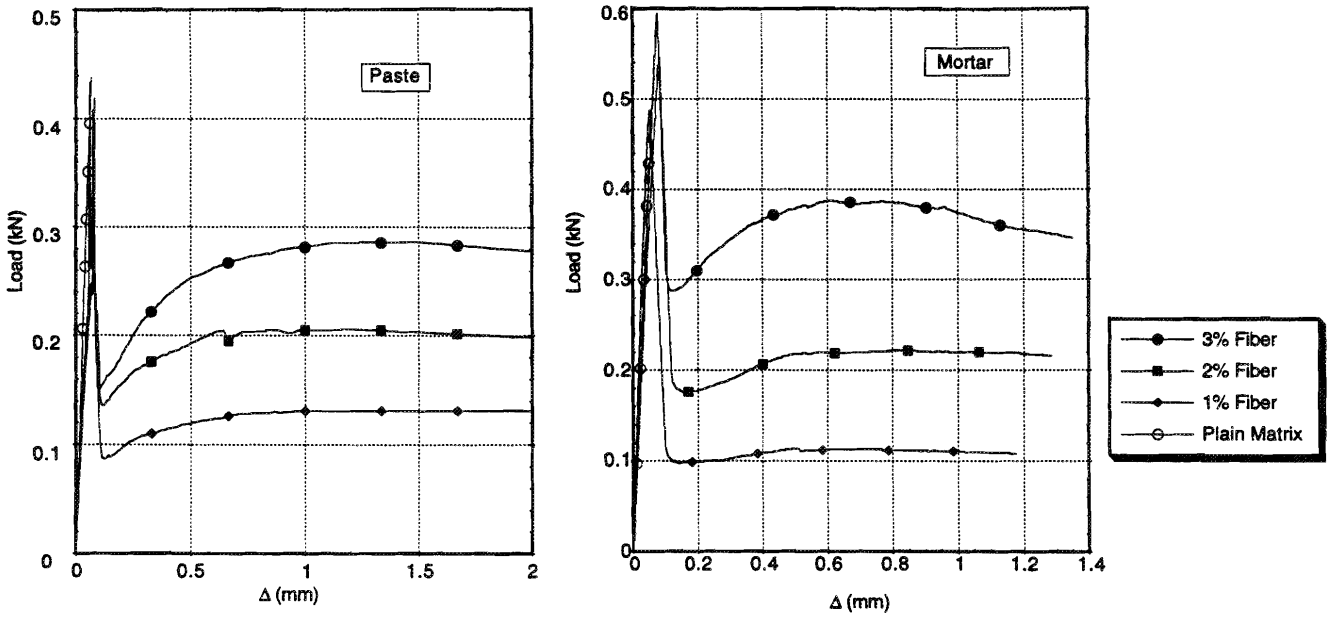

Table 1. Results from tests on unnotched beams.

	At bend over point			At peak		Total fracture	Strength		
Composite	Load (N)	Displacement (mm)	*E** (GPa)	Load (N)	Displacement (mm)	energy (N · m)	Flexural (MPa)	Tensile† (MPa)	Flexural/tensile ratio
P0	438	0.064	29.84	438	0.064	0.0145	5.60	2.96	1.89
PC1	456	0.067	29.67	486	0.126	0.1504	6.22	4.10	1.51
PC2	505	0.076	28.97	702	0.287	0.3348	8.98	6.10	1.47
PC3	625	0.071	38.38	718	0.377	0.5544	9.19	6.56	1.40
PS1	477	0.067	31.04	488	0.067	0.0672	6.24	4.40	1.41
PS2	639	0.082	33.97	649	0.081	0.1230	8.30	6.20	1.33
PS3	769	0.098	34.21	791	0.098	0.2040	10.12	7.32	1.38
PP1	458	0.065	30.72	458	0.065	0.2542	5.86	3.40	1.72
PP2	466	0.074	27.45	456	0.074	0.3882	5.83	3.55	1.64
PP3	482	0.086	24.43	464	0.086	0.5200	5.93	3.50	1.69
M0	475	0.065	31.86	475	0.065	0.0157	6.08	3.44	1.76
MC1	457	0.060	33.20	467	0.061	0.1307	5.97	4.75	1.25
MC2	500	0.097	22.47	622	0.347	0.3834	7.96	6.44	1.23
MC3	629	0.097	28.27	818	0.400	0.6418	10.47	7.10	1.47
MS1	617	0.074	35.91	641	0.080	0.1182	8.20	6.10	1.34
MS2	686	0.082	36.29	714	0.083	0.1861	9.13	7.21	1.26
MS3	748	0.097	33.97	750	0.094	0.2357	9.60	7.79	1.23
MP1	468	0.052	40.59	487	0.052	0.2349	6.23	4.20	1.48
MP2	524	0.062	36.84	546	0.063	0.4384	6.98	4.25	1.64
MP3	554	0.076	31.78	577	0.078	0.7250	7.38	4.35	1.69

*From $\Delta = 23PS^3/1296EI$ at bend over point (ignoring shear).

† From Part I of this paper.

In spite of these difficulties, various ways of dealing with the nonlinear effects in fracture of concrete have been proposed. These include the cohesive crack models (Hillerborg et al. 1976; Bazant and Oh 1983) and the effective crack models (Jenq and Shah 1985). In the cohesive crack models, a closing pressure is introduced at the tip of a propagating crack to characterize fracture; and in the effective crack models, linear elastic fracture mechanics is applied to an equivalent elastic or an effective crack.

In a fiber reinforced cement-based composite, along with the crack closing pressure due to aggregate interlocking in the matrix process zone ahead of a crack tip, fiber bridging occurs behind the crack tip to form what is commonly known as the fiber bridging zone. This makes the applications of

Fig. 7. Load vs. mid-span displacement (Δ) and load vs. crack mouth opening displacement (CMOD) plots for carbon fiber reinforced composite beams with a notch.

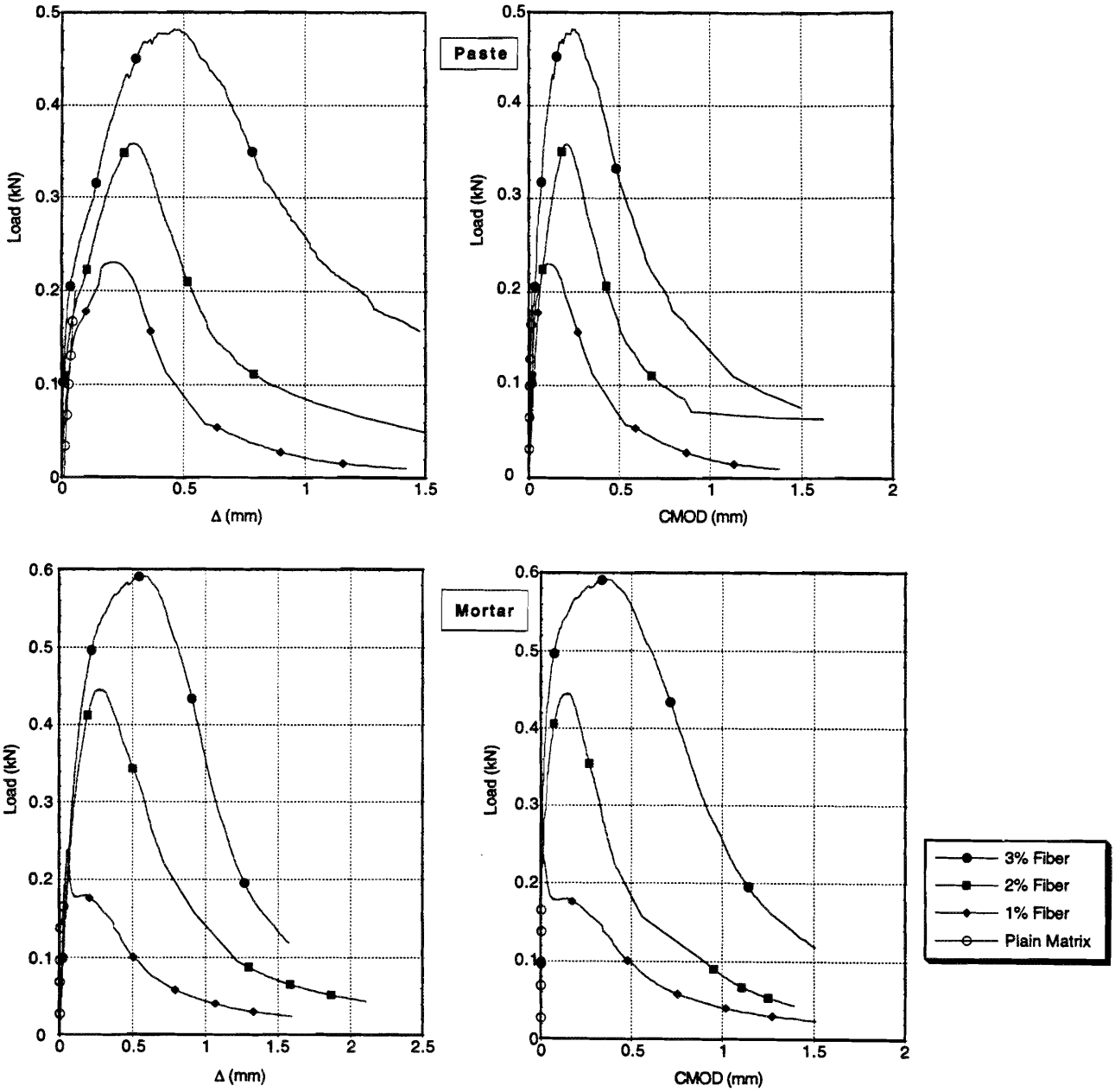

traditional linear elastic fracture mechanics even more questionable to fiber reinforced composites. Hillerborg extended the cohesive crack model to fiber reinforced concrete and related the closing pressure to fiber and interfacial characteristics (Hillerborg 1980). Closing pressure formulations in the fiber bridging zone were also developed by Visalvanich and Naaman (1983) and by Wecharatana and Shah (1983).

Another elastic-plastic fracture criterion called the J-integral has been successfully applied to metals (Hertzberg 1976). The J-integral (Rice et al. 1973) defines the stress conditions in the vicinity of a crack tip which can then be extended to those at the onset of critical propagation. Strictly speaking, therefore, J_C is a crack initiation — and not a crack propagation — criterion. This technique was adopted to characterize fiber reinforced concrete first by Mindess et al. (1977) and later by Li et al. (1987) who also obtained stress vs. crack separation curves from the J-integral plots. Ohgishi and Ono (1989) applied the analysis to polymer impregnated fiber reinforced mortars.

Finally, it is often argued that a single-parameter description of fracture based on K_C, or J_C, is not valid for cementitious materials and these materials in fact have an R-curve behavior (Visalvanich and Naaman 1991; Mai 1991; Karihaloo 1987; Mobasher et al. 1991). An R-curve, in principle, is a crack growth resistance curve and it plots the K or J values at the tip of a crack as a function of crack extension or crack opening. Considered to be a material property, an R-curve can be used to establish the conditions of fracture for

Fig. 8. Load vs. mid-span displacement (Δ) and load vs. crack mouth opening displacement (CMOD) plots for steel fiber reinforced composite beams with a notch.

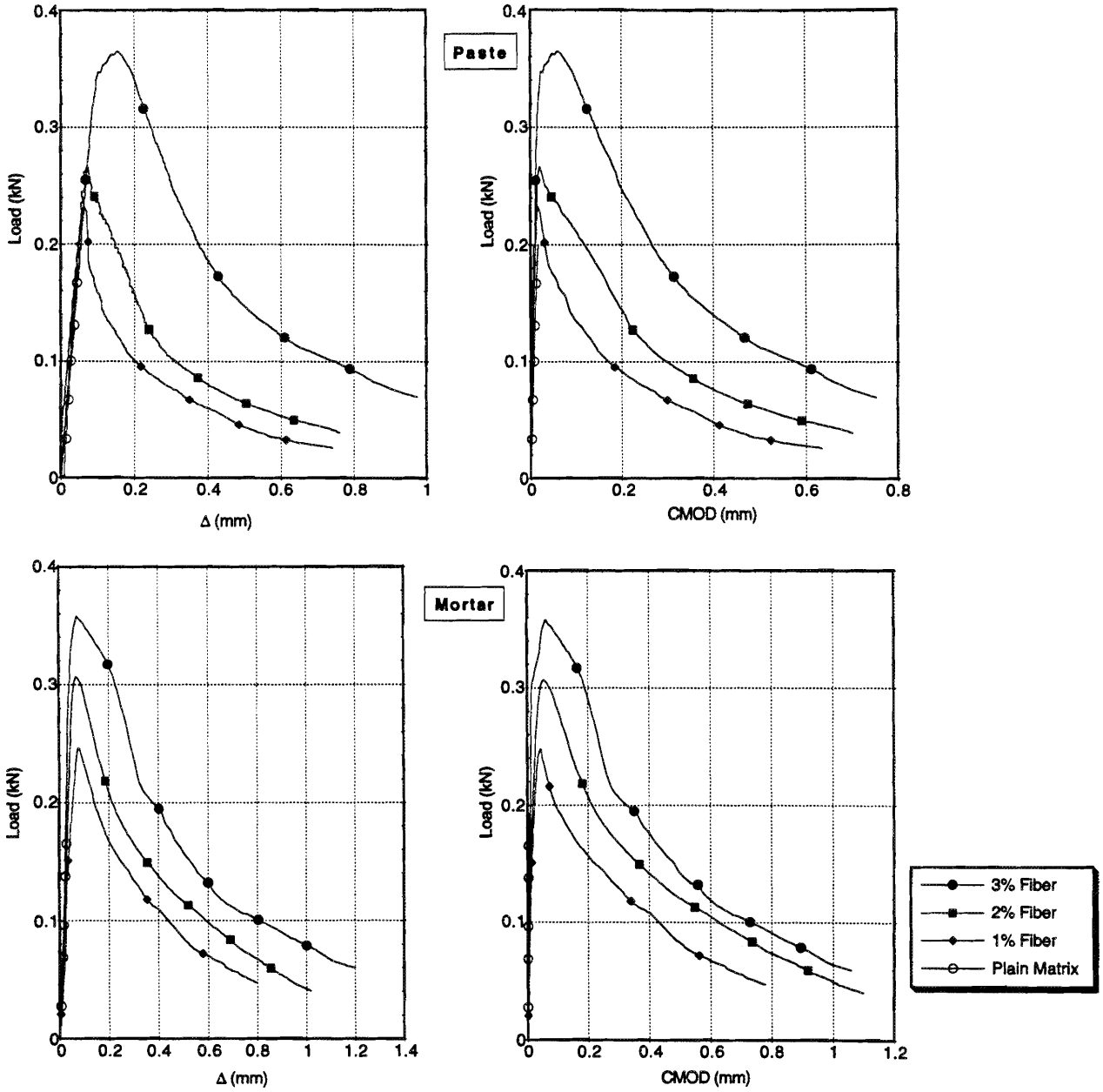

a given specimen geometry and loading configuration (McCabe 1973). The principles of *R*-curve analysis are shown in Fig. 1. If R^* is the crack driving force which is a characteristics of the structure, and R is the crack growth resistance which is an assumed materials property, then at fracture instability, the following two conditions have to be simultaneously satisfied:

$$[2] \quad R = R^*$$

$$[3] \quad \frac{\partial R}{\partial a} = \frac{\partial R^*}{\partial a}$$

This paper examines fracture in micro-fiber reinforced cement composites based on the various available technique of characterization.

Experimental program

Materials and mixes

The materials and mixes were described in details in Part I of this paper. In brief, two base matrices of cement paste (water:cement:silica fume = 0.35:1.00:0.20) and cement mortar (water:cement:silica fume:sand = 0.35:1.00:0.20:0.50) were reinforced with micro-fibers of carbon, steel, and polypropylene at volume fractions of 1%, 2%, and 3%. Silica fume was used in all mixes for an effective dispersion of fibers (Banthia 1992; Ohama 1989). Appropriate quantities of superplasticizer were added for proper workability, mouldability, finishability, and fiber dispersion. The mechanical properties and geometrical characteristics of fibers were as follows:

Fig. 9. Load vs. mid-span displacement (Δ) and load vs. crack mouth opening displacement (CMOD) plots for polypropylene fiber reinforced composite beams with a notch.

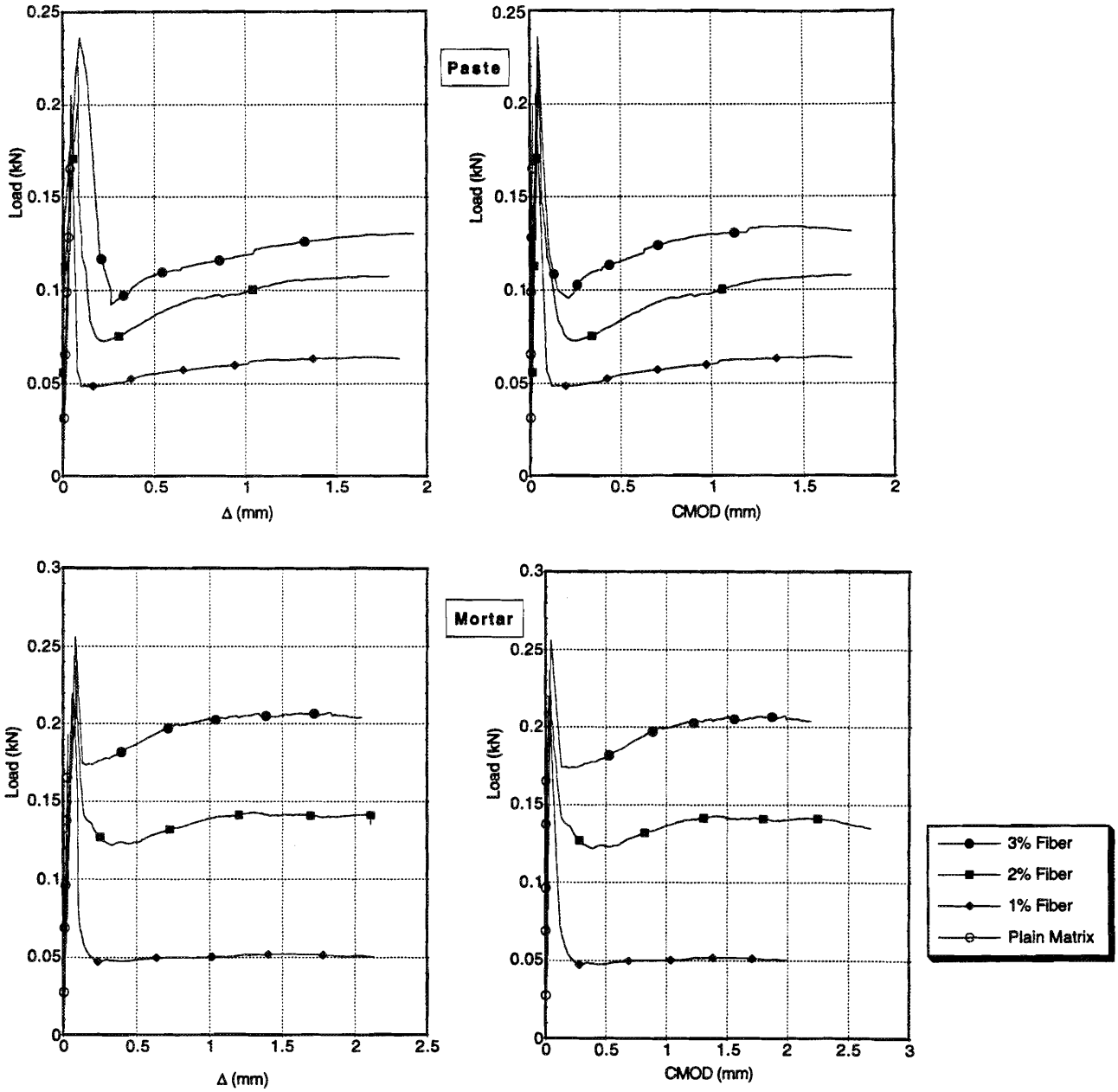

- Carbon fiber: 18 μm diameter, 6 mm long, E = 30 GPa, tensile strength = 590 MPa;
- Steel fiber: 25 μm × 5 μm section, 3 mm long, E = 200 GPa, tensile strength = 600 MPa;
- Polypropylene fiber: 4 μm diameter, 6 mm long, E = 1.41 GPa, tensile strength = 32 MPa.

Note that the fibers had widely different elastic moduli and strengths and had varyingly different surface characteristics such that the developed interfacial bond strengths with the matrices were also different.

Specimens and tests

Flexural specimens (25 mm × 25 mm × 225 mm) were cast using plexiglass moulds. One half of the specimens were left unnotched and in the other half of the specimen a 8 mm notch was cut using a fine saw. Both notched and unnotched specimens were tested in four-point bending (loading at third-points). A notched specimen during the test is shown in Fig. 2. Notice that a yoke is mounted around the specimen to eliminate the spurious deformations arising due to support settlements during a test. It has been shown previously that the use of a yoke is necessary to measure deflections comparable with the theoretical values (Banthia and Trottier 1994). As seen in Fig. 3, in the initial part of the curve, the displacements recorded using a yoke were somewhat smaller than those measured without one, which indicates that the yoke is capable of eliminating the spurious component of beam displacement occurring due to the settlement of supports themselves. In the unnotched specimens, beam dis-

placements at the center were monitored by placing an LVDT under the specimen. In the case of the notched specimens, in addition to beam centre-point displacements, crack opening displacements were also monitored by mounting an extensometer across the notch using grips installed on each side of the notch. The load was applied at a cross-arm speed of 0.01 mm/min for the plain specimens and at a rate of 0.02 mm/min for the fiber reinforced specimens to terminate the test in a reasonable amount of time. Tests took anywhere from 12 to 20 min. The data from the two extensometers and the load cell were acquired electronically using a data-logger running at 10 Hz.

Data analysis

The data comprise the applied load vs. beam mid-span displacement plots for the unnotched beams, and load vs. beam mid-span displacement plots and load vs. crack mouth opening displacement plots in the case of notched beams. While the plots for the unnotched beams were analyzed in a routine manner for strengths, fracture energies, etc., curves obtained for the notched specimens were analyzed as given in Appendix 2.

Results and discussion

Unnotched beams

The load–displacement curves for unnotched beams are given in Figs. 4, 5, and 6, respectively, for carbon, steel, and polypropylene fiber reinforced composites. These curves were analyzed to obtain the load and displacement at the bend over point (i.e., the point at which first nonlinearity in the load–displacement curve occurs), load and displacement at the ultimate load, and the total fracture energy to a displacement of 2.5 mm. The use of the yoke around the specimens as reported before (Banthia and Trottier 1994) allowed an accurate estimation of the displacements and hence permitted the calculation of the elastic modulus from the initial (linear) part of the curve. Ignoring shear deformations in the beam, the load and displacement values at the bend over point may be used to calculate the elastic moduli using the following equation:

$$[4] \quad \Delta = \frac{23PS^3}{1296EI}$$

where Δ is the beam mid-span displacement, P is the applied load, S is the span, and EI is the flexural rigidity.

Flexural strength (modulus of rupture) values were calculated from the ultimate loads using simple elastic analysis. It is recognized that such an approach is not entirely valid, given the nonlinear nature of these curves. The results of tests on unnotched beams are given in Table 1, where tensile strengths obtained from uniaxial tension tests reported previously in Part I of this paper are also included. Ratios of flexural-to-tensile strengths are also reported in Table 1.

Notice that in carbon–cement composites, an increase in fiber content led not only to an increase in the load carrying capacity but also to significant increases in the deformability or toughness. Steel fiber reinforcement also led to an improvement in the strength of the matrix, but the toughness improvements were not as pronounced as the carbon–cement composites. Finally, the presence of polypropylene fibers resulted in no increase in the strength, but the post-peak load

Fig. 10. Vertical displacements (Δ) plotted as a function of the crack tip opening displacement (CTOD) for the notched beams (mortar matrix): (*a*) carbon fiber reinforced composites; (*b*) steel fiber reinforced composites; and (*c*) polypropylene fiber reinforced composites.

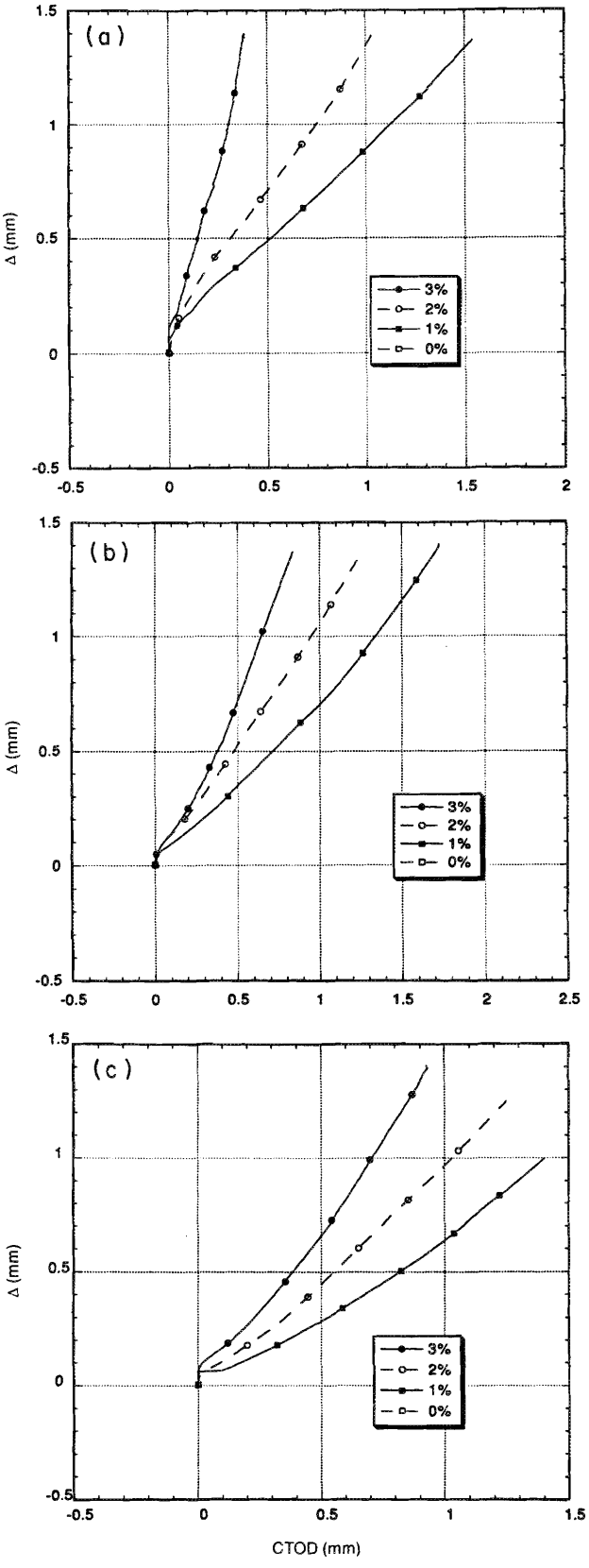

Table 2. Results from tests on notched beams.

	Conditions at the peak load								Conditions at unstable fracture (from K_R curves)		
Composite	P (N)	NSF*	Δ (mm)	CMOD† (mm)	CTOD‡ (mm)	K_{I,a_0}§ (MPa · m$^{1/2}$)	a_{eff}‖ (mm)	$K_{I,a_{eff}}$¶ (MPa · m$^{1/2}$)	K_{Ic} (MPa · m$^{1/2}$)	$CTOD_c$ (mm)	$CMOD_c$ (mm)
P0	199	0.45	0.0248	0.0167	0.0003	0.46	8.00	0.46	0.46	0.0003	0.0167
PC1	230	0.50	0.2130	0.1027	0.0334	0.53	9.43	0.62	0.92	0.1786	0.3034
PC2	358	0.70	0.2940	0.2093	0.1006	0.83	12.06	1.29	1.54	0.2112	0.3652
PC3	482	0.77	0.4610	0.2413	0.1202	1.12	12.55	1.84	2.33	0.3478	0.5722
PS1	232	0.48	0.0350	0.0170	0.0047	0.54	8.96	0.59	1.32	0.0862	0.1371
PS2	266	0.41	0.0720	0.0199	0.0058	0.62	9.08	0.69	1.78	0.1018	0.1633
PS3	364	0.47	0.0850	0.0605	0.0322	0.84	13.70	1.61	2.62	0.1412	0.2245
PP1	205	0.44	0.0450	0.0338	0.0052	0.47	8.27	0.40	0.47	0.0052	0.0338
PP2	220	0.47	0.0840	0.0466	0.0062	0.51	8.35	0.51	0.51	0.0062	0.0466
PP3	236	0.48	0.0930	0.0449	0.0065	0.54	8.44	0.55	0.54	0.0065	0.0449
M0	192	0.40	0.0360	0.0194	0.0005	0.45	8.03	0.45	0.45	0.0005	0.0194
MC1	238	0.52	0.0560	0.0117	0.0038	0.55	9.37	0.64	2.46	0.1849	0.2863
MC2	455	0.91	0.2750	0.1455	0.0830	1.06	15.94	2.72	3.40	0.1874	0.3007
MC3	591	0.93	0.5760	0.3326	0.2007	1.37	17.55	4.67	5.70	0.3867	0.6148
MS1	247	0.40	0.0420	0.0428	0.0144	0.57	9.55	0.67	1.45	0.1995	0.3166
MS2	306	0.44	0.0720	0.0500	0.0195	0.71	10.25	0.90	1.80	0.2218	0.3850
MS3	356	0.47	0.0800	0.0600	0.0314	0.83	13.39	1.40	2.74	0.3167	0.2211
MP1	219	0.46	0.0660	0.0269	0.0082	0.51	8.42	0.55	0.51	0.0082	0.0269
MP2	236	0.45	0.0830	0.0346	0.0147	0.55	9.16	0.55	0.55	0.0147	0.0346
MP3	255	0.46	0.0900	0.0452	0.0165	0.59	9.36	0.59	0.59	0.0165	0.0452

*Notch sensitivity factor, NSF = $[(P_{max})_{notched}]/[(P_{max})_{unnotched}]$.
†Crack mouth opening displacement (CMOD).
‡Crack tip opening displacement (CTOD) calculated from CMOD.
§Based on initial crack length a_0.
‖Calculated from compliance calibration.
¶Based on effective crack length, a_{eff}, at the peak load.

carrying capacity, hence the toughness, was improved. Improvements noticed above are also seen to be proportional to the fiber volume fraction. Similar behavior was observed in the case of composites tested in uniaxial tension (Banthia et al. 1994). There was no particular difference observed in the behaviors of the composites based on the mortar matrix and those based on the paste matrix. Flexural strengths for the various composites, as expected, were higher than their tensile strengths and the strength ratios (flexural-to-tensile) follow the trends usually reported by others (Wright 1955).

The elastic moduli calculated from the load and displacement values at the bend over point (eq. [2]), and reported in Table 1, fail to indicate any particular trend. Part of the reason is the general uncertainty regarding the exact location of the bend over point, which is often subject to human judgement errors. Notice also in Table 1 that the elastic moduli obtained from flexural tests are significantly higher than those obtained from uniaxial tensile tests. While the exact reasons behind this discrepancy are not clear, size effects, lack of certainty about the exact location of the bend over point, etc., may be cited as possible reasons. Also, since the values obtained in flexural tests compare well with those normally reported, possibly, some slippage at the grips occurred in the uniaxial tensile tests.

Notched beams

Experimental curves for the notched beams are given in Figs. 7–9. In these figures, applied load vs. beam mid-span displacement and applied load vs. crack mouth opening displacement (CMOD) plots are shown for carbon, steel, and polypropylene fiber reinforced composites based on paste and mortar matrices. In Fig. 10, beam mid-span displacements, Δ, are plotted against the crack tip opening displacements (crack tip opening displacement, CTOD, is geometrically related to the crack mouth opening displacement, CMOD, as outlined in Appendix 2) for carbon, steel, and polypropylene fiber reinforced mortars, respectively. Notice that as the fiber volume fraction is increased, there is a decrease in the CTOD values at a given beam displacement. This is a direct indication of the more effective crack bridging rendered by fibers when present in the composite at a higher volume fraction. Note also that the CTOD values at a given fiber volume fraction are greater for polypropylene fiber reinforced composite than for those reinforced with steel or carbon fibers. This may be a direct consequence of the lower modulus of elasticity of polypropylene fibers than carbon or steel fibers and also an indicative of the poor bond developed in this case.

Using Appendix 2, the data for the notched beams were analyzed and the results are given in Table 2. In particular, the following conditions at the peak load are reported: the load, the beam displacement, CMOD, CTOD, fracture toughness based on initial crack length (K_{I,a_0}), the effective crack length (a_{eff}), obtained using compliance calibration, and the fracture toughness based on the effective crack length ($K_{I,a_{eff}}$). Also given in Table 2 are the notch sensitivity fac-

Fig. 11. K_R-curves for carbon fiber reinforced composites plotted as crack growth resistance (K_I vs. a_{eff}) and crack opening resistance (K_I vs. CTOD) curves.

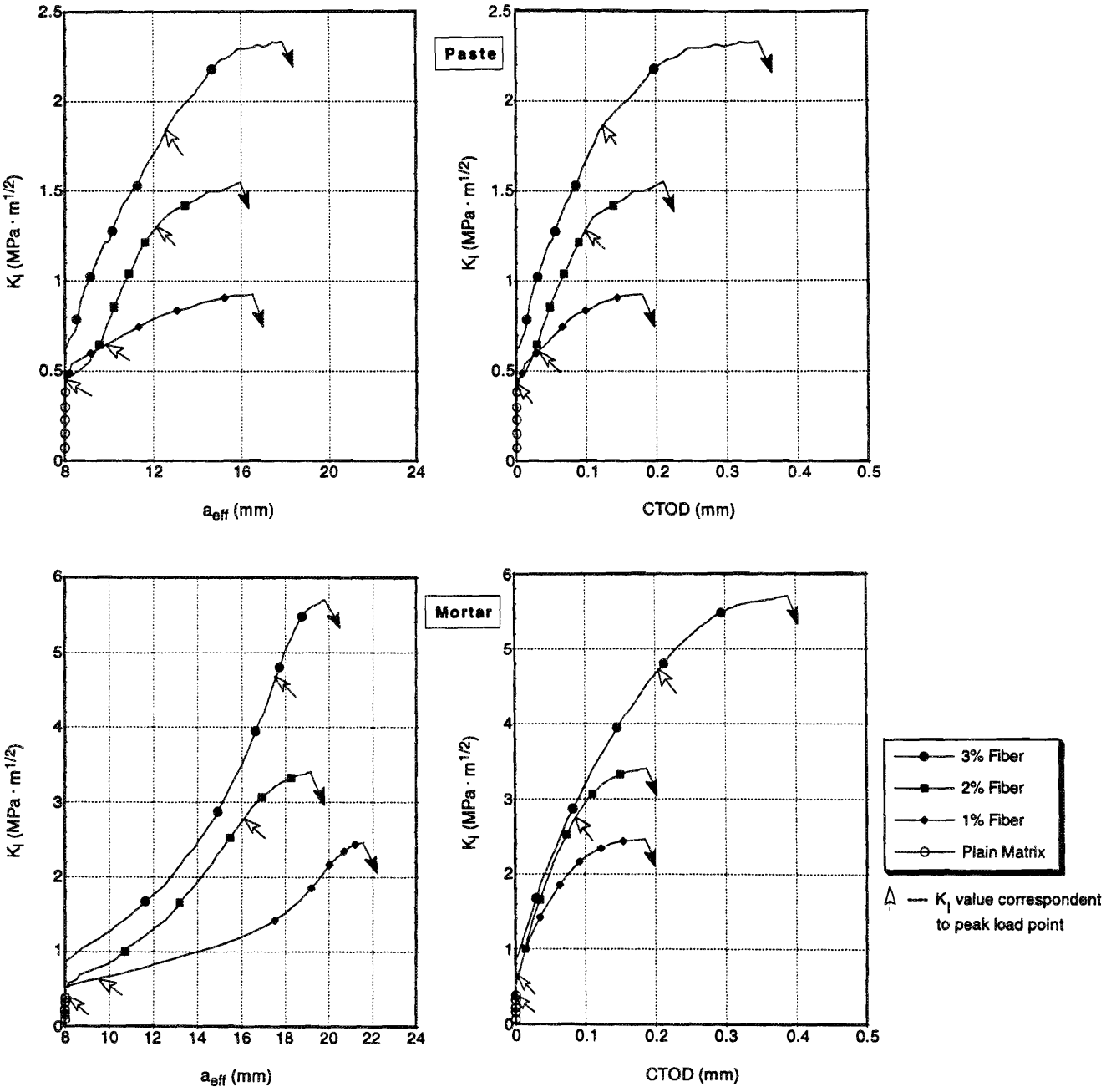

tors defined as the ratio of peak load supported by a notched beam to that supported by an unnotched beam of the same material. As expected, notched beams supported reduced ultimate loads and this reduction was more pronounced for steel and polypropylene fiber reinforced composites as compared to carbon fiber reinforced composites. This is related to the superior fracture toughness of carbon fiber reinforced composites as discussed later. Notice also that while the curves for the notched beams have, in general, shapes similar to those for the unnotched beams, the brittleness observed in steel fiber reinforced unnotched beams is not as pronounced in the notched beams. Fracture toughness values based on the initial length of the crack (a_0), K_{I,a_0}, indicate the superior fracture toughness of carbon and steel micro-fiber reinforced composites. However, based on fracture toughness values calculated using the modified crack lengths (a_{eff}), $K_{I,a_{eff}}$, the very high fracture toughness of carbon fiber reinforced mortars over all other composites becomes noticeable.

As discussed before, a single-parameter representation of fracture in cement-based materials is questionable. Instead, therefore, a crack growth resistance curve (R-curve) is preferred where the crack growth resistance, expressed as the apparent stress intensity factor, K_I, at the tip of a crack, is plotted as a function of crack length or crack extension. It is proposed that such an R-curve may be treated as a material constant (Fig. 1). In Figs. 11, 12, and 13, crack growth resistance curves are given for carbon, steel, and polypropylene fiber reinforced composites, where K_I values are plot-

Fig. 12. K_R-curves for steel fiber reinforced composites plotted as crack growth resistance (K_I vs. a_{eff}) and crack opening resistance (K_I vs. CTOD) curves.

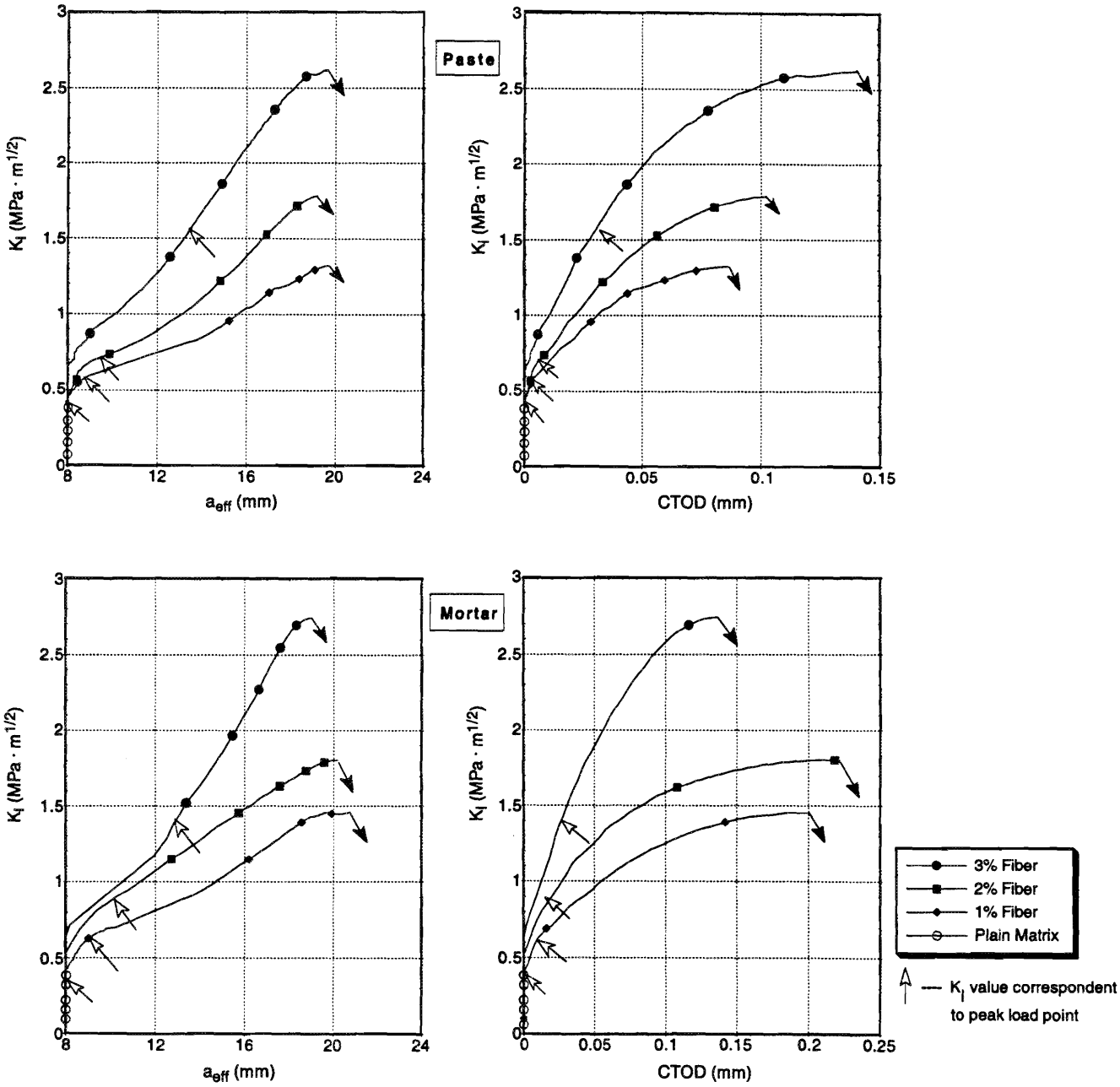

ted as a function of a_{eff}. Notice that for carbon and steel fiber reinforced composites, the peak value of K_I occurs not at the peak load but *after* the peak load. In Table 2, the peak value of K_I regardless of where it is on the crack growth resistance curves is noted as K_{IC} (the true fracture toughness). The higher values of K_{IC} for the carbon fiber reinforced composites than for other composites indicate, once again, the significantly high fracture resistance of these composites. It is worth noticing that the engineering properties obtained in a conventional manner using unnotched beams (Table 1) fail to recognize this important feature of carbon fiber reinforced composites.

The K_R-curves in Figs. 11–13 were plotted as a function of a_{eff} obtained from the compliance calibration. However, as shown in Fig. 14 a crack rarely takes a straight path and the tortuous path taken by the crack diminishes the validity of a crack growth resistance curve. Alternatively, one can replot the stress intensity factors at the crack tip as a function of the crack tip opening displacement (CTOD) instead of the effective crack length. In this regard, it is believed that while the applied load and the effective crack length rapidly approach a limiting value during a test, crack opening displacement values approach failure conditions in a relatively stable manner (Hertzberg 1976). Based on these reasons, one can argue that plots of K_I vs. CTOD may be a more reasonable way of characterizing these composites. Such curves, termed the crack opening resistance curves, are also shown in Figs. 11–13. Clearly, the calculation of K_I still

Fig. 13. K_R-curves for polypropylene fiber reinforced composites plotted as crack growth resistance (K_I vs. a_{eff}) and crack opening resistance (K_I vs. CTOD) curves.

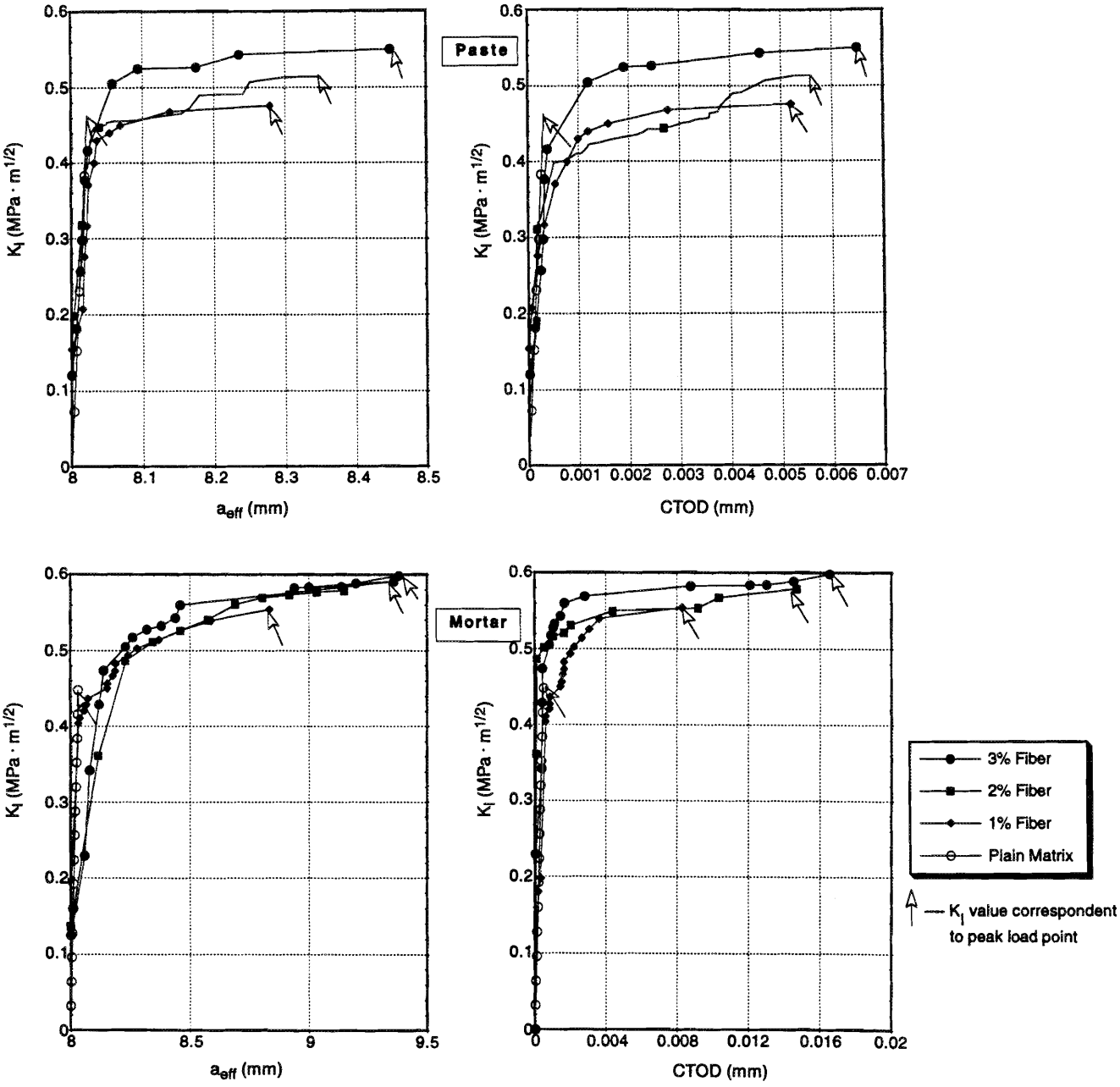

involves estimating a_{eff} from compliance calibration such that K_I carries all the inaccuracies of this type of analysis, and the peak value of K_I in the crack opening resistance curves is not any different from that in the crack growth resistance curves.

One additional outcome of the crack opening resistance curves is the critical value of the crack tip opening displacement, $CTOD_c$, occurring at the peak value of K_I, which in itself can be treated as a fracture criterion. These values are noted in Table 2 along with the corresponding values of the $CMOD_c$ for the various composites. It is to be recognized, however, that the values of $CTOD_c$ reported in Table 2 are a function of the specimen geometry and not a fundamental property of the composites (Hertzberg 1976). Also, $CTOD_c$ values for the various composites are not only a function of the fiber length but also of the strength of the interfacial bond.

Research challenges in micro-fiber reinforced cement composites

Micro-fiber reinforced cement composites are an exciting new development in fiber reinforced cement-based materials. Need exists to fully understand the micromechanical aspects of fracture in these composites such that the fiber-matrix interaction in the pseudo-strain-hardening regime can be analyzed and composites can be optimized. Equally important is to understand the physical and durability characteristics of these composites. Proper manufacturing and processing of

Fig. 14. Micrograph showing the tortuous path taken by a crack in polypropylene fiber reinforced composite.

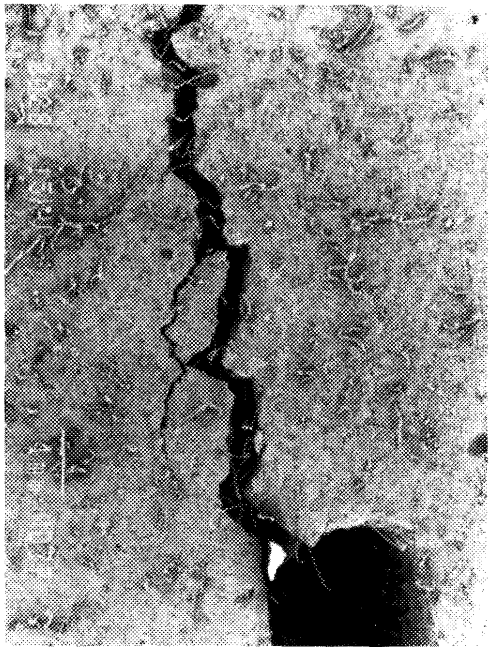

these composites is also a challenge; manufacturing techniques such as extrusion, pressure moulding, along with specialized curing techniques have to be developed. Finally, need exists to evaluate the performance of these composites when in an actual applications.

Concluding remarks

This and the previous paper (Part I) examine the improvements in the tensile strength and fracture toughness of cement-based materials reinforced with a high volume fraction of carbon, steel, and polypropylene micro-fibers. In this paper, tests on notched and unnotched beams were conducted, which led not only to the engineering properties but also to crack growth resistance curves and crack opening resistance curves plotted in terms of the stress intensity factor, K, at the crack tip. These K_R-curves indicate the exceptionally high fracture toughness of carbon fiber reinforced composites over the other composites and provide a valuable insight into the toughening mechanisms that exist in these composites. Significant research is still needed, however, to identify the experimental factors which influence the curve itself and to model the curve in terms of fiber, matrix, and interfacial properties.

Acknowledgments

The continued support of the Natural Sciences and Engineering Research Council of Canada is gratefully acknowledged. Thanks are also due to Novocon International, Fibrin, Inc., and Kreha Corporation of America for supplying the fibers.

References

Balaguru, P.N., and Shah, S.P. 1992. Fiber reinforced cement composites. McGraw-Hill Inc., New York.

Banthia, N. 1992. Pitch-based carbon fiber reinforced cements: structure, performance, applications and research needs. Canadian Journal of Civil Engineering, **19**(1): 26–38.

Banthia, N., and Dubeau, S. 1994. Steel and carbon micro-fiber reinforced cement-based materials for thin repairs. ASCE Journal of Materials in Civil Engineering, **6**(1): 88–99.

Banthia, N., and Trottier, J.-F. 1995. Test methods for flexural toughness characterization of fiber reinforced concrete: some concerns and a proposition. ACI Materials Journal, **92**(1): 48–57.

Banthia, N., Djeridane, S., and Pigeon, M. 1992. Electrical resistivity of cements reinforced with micro-fibers of carbon and steel. Cement and Concrete Research, **22**(5): 804–814.

Banthia, N., Azzabi, M., and Pigeon, M. 1993. Restrained shrinkage cracking in fiber reinforced cementitious composites. Materials and Structures RILEM (Paris), **26**(161): 405–413.

Banthia, N., Moncef, A., Chokri, K., and Sheng, J. 1994. Micro-fiber reinforced cement composites. I. Uniaxial tensile response. Canadian Journal of Civil Engineering, **21**(6): 999–1011.

Bazant, Z.P., and Oh, B.H. 1983. Crack band theory for fracture of concrete. Materials and Structures, **16**(83): 155–177.

Beaudoin, J.J. 1991. Microstructural modifications of macro and micro-fiber reinforced hydrated portland cement matrices. Proceedings of the 1st Canadian University–Industry Workshop on Fiber Reinforced Concrete, Québec, Que. *Edited by* N. Banthia. pp. 129–139.

Bentur, A., and Mindess, S. 1990. Fiber reinforced cementitious composites. Elsevier Applied Science Publishers, London and New York.

Dugdale, D.S. 1960. Journal of Mechanics and Physics of Solids, **8**: 100.

Hertzberg, R.W. 1976. Deformation and fracture mechanics of engineering materials. John Wiley and Sons, New York.

Hillerborg, A. 1980. Analysis of fracture by means of the fictitious crack model, particularly for fiber reinforced concrete. Journal of Cement Composites and Lightweight Concrete, **2**: 177–184.

Hillerborg, A., Modeer, M., and Peterson, P.-E. 1976. Analysis of crack formation and crack growth in concrete by means of fracture mechanics and finite elements. Cement and Concrete Research, **6**: 773–782.

Irwin, G.R. 1958. Handbuch der physik. Vol. VI. Springer, Berlin, Germany.

Jenq, Y.S., and Shah, S.P. 1985. Two parameter fracture model for concrete. ASCE Journal of Engineering Mechanics Division, **111**(10): 1227–1241.

Karihaloo, B.L. 1987. Do plain and fiber reinforced concretes have an R-curve behavior? Proceedings, SEM-RILEM International Conference on Fracture of Concrete and Rock, Houston, Tex., pp. 128–137.

Li, V.C., Chan, C.-M., and Leung, C.K.Y. 1987. Experimental determination of the tension-softening relations for cementitious composites. Cement and Concrete Research, **17**: 441–452.

Mai, Y.-M. 1991. Failure characterization of fiber reinforced cement composites with R-curve characteristics. *In* Toughening mechanisms in quasi-brittle materials. *Edited by* S.P. Shah. Kluwer Academic Publishers, The Netherlands, pp. 467–505.

McCabe, D.E. (*Editor*). 1973. Fracture toughness evaluation by R-curve methods. American Society for Testing and Materials, Philadelphia, Pa., ASTM-STP 527.

Mindess, S. 1991. The fracture process zone in concrete. *In* Toughening mechanisms in quasi-brittle materials. *Edited by* S.P. Shah. Kluwer Academic Publishers, The Netherlands, pp. 271–286.

Mindess, S., Lawrence, F.W., and Kesler, C.E. 1977. The J-integral as a fracture criterion for fiber reinforced concrete. Cement and Concrete Research, **7**: 731–742.

Mobasher, B., Ouyang, C., and Shah, S.P. 1991. Modeling of fiber

toughening in cementitious materials using and R-curve approach. International Journal of Fracture, **50**: 199–219.

Ohama, Y. 1989. Carbon–cement composites. Carbon, **27**(5): 729–737.

Ohgishi, S., and Ono, H. 1989. Non-linear fracture toughness (J_{IC}, G_F) of inorganic polymer impregnated cement mortar reinforced by new material fiber. *In* Fracture of concrete and rock: recent developments. *Edited by* S.P. Shah, S.E. Swartz, and B. Barr. Elsevier Applied Science Publishers, London and New York, pp. 71–80.

Ouyang, C., and Shah, S.P. 1992. Toughening of high strength cementitious matrix reinforced by discontinuous short fibers. Cement and Concrete Research, **22**: 1201–1215.

Rice, J.R., Paris, P.C., and Merkle, J.G. 1973. Progress in flaw growth and fracture toughness testing. American Society for Testing and Materials, Philadelphia, Pa., pp. 231–245, ASTM STP 536.

Swamy, R.N. 1979. Fracture mechanics applied to concrete. *In* Developments in concrete technology. I. *Edited by* F.D. Lydon. Applied Science Publishers, Ltd., pp. 221–281.

Tada, H., Paris, P.C., and Irwin, G.R. 1985. The stress analysis of cracks handbook. Del Research Corp., Hellertown, Pa.

Visalvanich, K., and Naaman, A.E. 1983. Fracture model for fiber reinforced concrete. ACI Journal, March–April, pp. 128–138.

Visalvanich, K., and Naaman, A.E. 1991. Fracture methods in cement composites. ASCE Journal of Engineering Mechanics Division, **107**(EM6): 1155–1171.

Wecharatana, M., and Shah, S.P. 1983. A model for predicting fracture resistance of fiber reinforced concrete. Cement and Concrete Research, **13**: 819–829.

Wright, P.J.F. 1955. Comment on an indirect tensile test on concrete cylinders. Magazine of Concrete Research (London), **7**(20): 87–96.

Appendix 1. List of symbols

a	crack length
a_0	initial crack (notch) length
a_{eff}	effective crack length ($\geq a_0$)
b	width of the beam
c	compliance = CMOD/P
$c(a_0)$	initial compliance
$c(a_{eff})$	compliance at a crack length a_{eff} ($>a_0$)
d	depth of the beam
d'	depth from the bottom of the beam at which crack mouth opening displacement is measured
M	moment
P	applied load
S	span
$\alpha(a)$	$= (a + d')/(d + d')$
$\alpha(a_0)$	$= (a_0 + d')/(d + d')$
$\alpha(a_{eff})$	$= (a_{eff} + d')/(d + d')$
Δ	midspan displacement
σ	flexural stress

Appendix 2. Analysis of notched beams

(1) Effective crack length, a_{eff}

Crack mouth opening displacement, CMOD, is given by Tada et al. (1985)

$$[A1] \quad \text{CMOD} = \frac{6\sigma a}{E} V_1[\alpha(a)]$$

where

Fig. A1. Details of a notched beam under load.

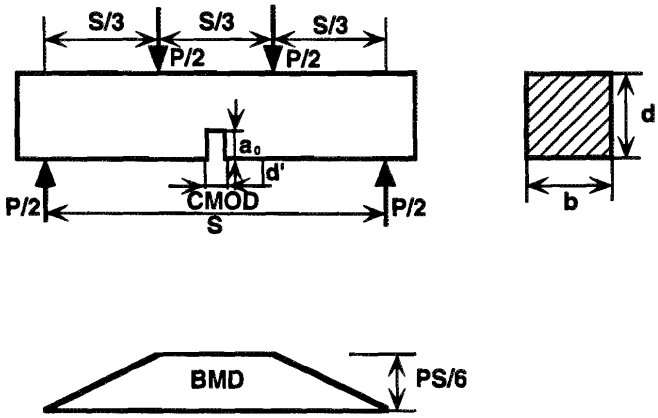

Fig. A2. Compliance calibration in a notched beam.

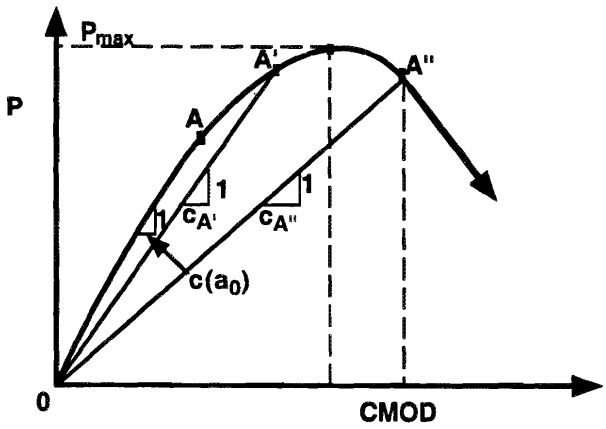

$$V_1[\alpha(a)] = 0.8 - 1.7\alpha(a) + 2.4\alpha^2(a) + 0.66/[1 - \alpha^2(a)]$$

For a beam under third-point loading (Fig. A1),

$$[A2] \quad \sigma = \frac{PS}{bd^2}$$

From [A1] and [A2],

$$[A3] \quad E = 4\left(\frac{P}{\text{CMOD}}\right)\left(\frac{aS}{bd^2}\right) V_1[\alpha(a)]$$

Writing [A3] at the bend over point A (Fig. A2),

$$[A4] \quad E = \frac{4}{c(a_0)} \frac{a_0 S}{bd^2} V_1[\alpha(a_0)]$$

and at any other point A′ or A″ in Fig. A2,

$$[A5] \quad E = \frac{4}{c(a_{eff})} \frac{a_{eff} S}{bd^2} V_1[\alpha(a_{eff})]$$

From [A4] and [A5],

$$a_{eff} = \frac{c(a_{eff})}{c(a_0)} a_0 \frac{V_1[\alpha(a_0)]}{V_1[\alpha(a_{eff})]}$$

(2) Stress intensity factor, $K_I(a)$

$$K_I(a) = \sigma\sqrt{\pi a}\, F_1(a/d)$$

where

$$F_1(a/d) = 1.122 - 1.40(a/d) + 7.33(a/d)^2 - 13.08(a/d)^3 + 14.0(a/d)^4$$

and σ is given by [A2].

(3) Crack tip opening displacement, CTOD

$$\text{CTOD} = \text{CMOD} \times Z[\alpha(a), \beta(a)]$$

where

$$\alpha(a) = a/d, \qquad \beta(a) = a_0/a$$

and

$$Z[\alpha(a), \beta(a)] = [(1 - \beta(a))^2 + (1.081 - 1.49\alpha(a)) \times (\beta(a) - \beta^2(a))]^{1/2}$$